Quantifying mixing in viscously unstable porous media flows

Birendra Jha, Luis Cueto-Felgueroso, and Ruben Juanes*
Massachusetts Institute of Technology, 77 Massachusetts Avenue, Building 48, Cambridge, Massachusetts 02139, USA
(Received 5 August 2011; revised manuscript received 22 October 2011; published 16 December 2011)

Viscous fingering is a well-known hydrodynamic instability that sets in when a less viscous fluid displaces a more viscous fluid. When the two fluids are miscible, viscous fingering introduces disorder in the velocity field and exerts a fundamental control on the rate at which the fluids mix. Here we analyze the characteristic signature of the mixing process in viscously unstable flows, by means of high-resolution numerical simulations using a computational strategy that is stable for arbitrary viscosity ratios. We propose a reduced-order model of mixing, which, in the spirit of turbulence modeling and in contrast with previous approaches, recognizes the fundamental role played by the mechanical dissipation rate. The proposed model captures the nontrivial interplay between channeling and creation of interfacial area as a result of viscous fingering.

DOI: 10.1103/PhysRevE.84.066312 PACS number(s): 47.51.+a, 47.56.+r, 47.20.Gv

I. INTRODUCTION

Mixing of fluids is an important and complex phenomenon. Several chemical [1], pharmaceutical [2,3], and food processing [4] operations require controlled mixing of fluids at low Reynolds numbers, a notoriously difficult problem [5–7]. Mixing also plays a fundamental role in natural processes, including groundwater flows in heterogeneous media [8], mantle convection [9,10], debris gravity currents [11], population genetics [12,13], mammalian digestion [14], and bacterial locomotion [15–21].

When the physical properties of the fluids, such as density or viscosity, are sufficiently different, mixing may become heavily influenced by the formation of hydrodynamic instabilities. It has been shown, under controlled conditions, that such instabilities can speed up the mixing process enormously [22,23]. Recently, we have shown that miscible viscous fingering [24]—the hydrodynamic instability that ensues between two fully miscible fluids when the least viscous fluid displaces the most viscous one—can be employed as an agent for enhanced mixing at low Reynolds numbers [25].

Miscible viscous fingering has been studied extensively in the past through laboratory experiments [26–28] and numerical simulations [29–33]. Linear stability analyses have explained the onset and growth of instabilities as a function of the viscosity contrast and the flow rate for rectilinear [34] and radial [35] geometries. A number of experimental, theoretical, and numerical studies have been carried out to understand the effects of anisotropic dispersion [32,36,37], medium heterogeneity [38–41], gravity [42–47], chemical reaction [48–51], adsorption [52], and flow configuration [53–58] on the viscous fingering instability.

It has long been recognized that viscous fingering leads to enhanced *spreading* of the displacing fluid [59,60]. A large body of literature, going back to the works of Koval [61] and Todd and Longstaff [62], has focused on the development of fractional flow formulations to predict averaged concentrations and breakthrough curves [63–73].

Despite the considerable work done, the effect of viscous fingering on fluid *mixing* remains unexplored. In this article, we present the derivation of an upscaled model to quantify the degree of mixing in a viscously unstable displacement. We present a numerical scheme for the high-resolution simulation of the viscous fingering process with arbitrary viscosity contrast. This scheme is stable for arbitrarily high viscosity contrasts, for which the traditional schemes become unstable. Based on the results of high-resolution numerical simulation and scaling arguments that reflect the dissipative properties of the flow, we formulate a mixing model that, in the spirit of turbulence modeling, quantifies the decay of concentration variance and the evolution of mean scalar dissipation rate [25].

II. GOVERNING EQUATIONS

We consider Darcy flow of two fluids of different viscosities μ_1 and μ_2, where $\mu_1 < \mu_2$, in a porous medium. We assume that the porosity ϕ (volume of voids per unit volume of porous medium) and the scalar permeability k (coefficient relating flow velocity and pressure gradient) are uniform and constant. This means that the porous medium is homogeneous and isotropic. The two fluids are assumed to be first-contact miscible, neutrally buoyant, and incompressible. This means that the injected and the resident fluids mix instantaneously in all proportions to form a single phase and, therefore, surface tension effects are, by definition, absent. The diffusivity D between the fluids is assumed to be constant, isotropic, and independent of concentration. The length and width of the domain are L and W, and the mean velocity is in the x direction and of magnitude U. The governing equations in dimensional form are

$$\phi \frac{\partial c}{\partial t} + \nabla \cdot (\boldsymbol{u} c - D \nabla c) = 0, \tag{1}$$

$$\boldsymbol{u} = -\frac{k}{\mu(c)} \nabla p, \quad \nabla \cdot \boldsymbol{u} = 0, \tag{2}$$

in $x \in [0, L]$ and $y \in [0, W]$. Equation (1) is a linear advection-diffusion transport equation (ADE) for the concentration of the less viscous fluid $c(\boldsymbol{x}, t)$, that is, the mass of the less viscous fluid per unit volume of the mixture. Equation (2) is Darcy's law defining the velocity of the mixture, which satisfies the incompressibility constraint. The viscosity of the mixture, $\mu(c)$, is assumed to be an exponential function

*juanes@mit.edu

of concentration, $\mu(c) = \mu_1 e^{R(1-c)}$, where $R = \log M$ and $M = \mu_2/\mu_1$ is the viscosity ratio.

We express the equations in nondimensional form using characteristic quantities, W, U, and $\mu_2 = \mu_1 e^R$, for length, velocity, and viscosity, respectively. The characteristic time and pressure drop are given by $T = \phi W/U$ and $P = \mu_2 U W/k$, respectively. Abusing notation, we write the governing equations in dimensionless form:

$$\frac{\partial c}{\partial t} + \nabla \cdot \left(\boldsymbol{u} c - \frac{1}{\mathrm{Pe}} \nabla c \right) = 0, \tag{3}$$

$$\boldsymbol{u} = -\frac{1}{\mu(c)} \nabla p, \quad \nabla \cdot \boldsymbol{u} = 0, \tag{4}$$

in $x \in [0, L/W]$, $y \in [0,1]$, where $c \in [0,1]$ is now the volume fraction of the least viscous fluid, and $\mu(c) = e^{-Rc}$ is the dimensionless viscosity. Darcy's law and the divergence-free condition in Eq. (4) can be combined to obtain the pressure equation in explicit form,

$$\nabla \cdot \left(-\frac{1}{\mu(c)} \nabla p \right) = 0. \tag{5}$$

The system is governed by two nondimensional groups: the Péclet number $\mathrm{Pe} = UW/D$ and the viscosity ratio $M = \mu_2/\mu_1$.

A. Fluid mixing in a periodic field

We use the global variance of the concentration field, $\sigma^2 \equiv \langle c^2 \rangle - \langle c \rangle^2$, to define the degree of mixing,

$$\chi(t) = 1 - \sigma^2(t)/\sigma^2_{\max}, \tag{6}$$

where $\langle \cdot \rangle$ denotes spatial averaging over the domain volume V. The maximum variance, $\sigma^2_{\max}$, corresponds to a perfectly segregated state, hence $\sigma^2_{\max} = 0.25$ for a mean concentration $\langle c \rangle = 0.5$. In a perfectly mixed state, $\sigma^2 = 0$ and $\chi = 1$.

We first derive the evolution equation for the global concentration variance σ^2. Multiplying the ADE [Eq. (3)] by c results in

$$c \frac{\partial c}{\partial t} + c \nabla \cdot (\boldsymbol{u} c) = \frac{1}{\mathrm{Pe}} c \nabla^2 c, \tag{7}$$

where ∇^2 denotes the Laplacian operator. Expanding the right-hand side and averaging over the domain,

$$\frac{1}{2} \left\langle \frac{\partial c^2}{\partial t} + \nabla \cdot (\boldsymbol{u} c^2) \right\rangle = \frac{1}{\mathrm{Pe}} \langle \nabla \cdot (c \nabla c) - |\nabla c|^2 \rangle. \tag{8}$$

Applying the Gauss divergence theorem gives

$$\begin{aligned} \langle \nabla \cdot (\boldsymbol{u} c^2) \rangle &= \frac{1}{V} \int_S c^2 \boldsymbol{u} \cdot \boldsymbol{n} \, dS, \\ \langle \nabla \cdot (c \nabla c) \rangle &= \frac{1}{V} \int_S c \nabla c \cdot \boldsymbol{n} \, dS, \end{aligned} \tag{9}$$

where S is the surface bounding V, dS the element of boundary area, and $\boldsymbol{n}$ the outward-pointing normal to the boundary. Assuming periodicity in x and y, these two boundary surface integrals vanish and Eq. (8) becomes

$$\frac{d\langle c^2 \rangle}{dt} = -\frac{2}{\mathrm{Pe}} \langle |\nabla c|^2 \rangle. \tag{10}$$

Since the mean concentration $\langle c \rangle$ remains constant in a periodic domain, the evolution of concentration variance under periodic boundary conditions becomes [74,75]

$$\frac{d\sigma^2}{dt} = -2\epsilon, \tag{11}$$

where $\epsilon \equiv \langle |\nabla c|^2 \rangle / \mathrm{Pe}$ is the dimensionless mean scalar dissipation rate. In absence of any source terms, Eq. (11) indicates that the global concentration variance monotonically decays with time due to the dissipative action of ϵ, which is positive as long as there are gradients in the concentration field. Physically, ϵ can be interpreted as a mixing rate or, equivalently, as a rate at which scalar fluctuations are destroyed.

Equation (11) motivates us to study the evolution of ϵ in time and understand its dependence on the physical parameters, R and Pe. Taking the gradient of the ADE in Eq. (3) and then dot product with ∇c yields

$$\nabla c \cdot \frac{\partial \nabla c}{\partial t} + \nabla c \cdot \nabla (\boldsymbol{u} \cdot \nabla c) = \frac{1}{\mathrm{Pe}} \nabla c \cdot \nabla (\nabla^2 c), \tag{12}$$

Denoting $\boldsymbol{g} = \nabla c$ and using $\nabla \cdot \boldsymbol{u} = 0$,

$$\begin{aligned} &\frac{1}{2} \frac{\partial |\nabla c|^2}{\partial t} + \sum_{i,j} \frac{\partial u_i}{\partial x_j} g_i g_j + \frac{1}{2} \sum_i \nabla \cdot \left(\boldsymbol{u} g_i^2 \right) \\ &\quad = \frac{1}{\mathrm{Pe}} \nabla c \cdot \nabla (\nabla^2 c), \end{aligned} \tag{13}$$

where u_i, x_j, and g_i are components of the velocity, position, and concentration gradient vectors, respectively. Integrating over a periodic domain removes the divergence terms on the left-hand side. Expanding the right-hand side,

$$\begin{aligned} \nabla c \cdot \nabla (\nabla^2 c) &= \sum_{i,j} g_i \frac{\partial^2 g_j}{\partial x_i \partial x_j} = \sum_{i,j} g_i \frac{\partial^2 g_i}{\partial x_j^2} \\ &= \sum_i \nabla \cdot (g_i \nabla g_i) - \sum_{i,j} \left(\frac{\partial g_i}{\partial x_j} \right)^2. \end{aligned} \tag{14}$$

Upon volume integration, the divergence terms in Eqs. (13) and (14) vanish under periodic boundary conditions. Using the definition of ϵ, Eq. (13) becomes

$$\frac{d\epsilon}{dt} + \frac{2}{\mathrm{Pe}} \sum_{i,j} \left\langle \frac{\partial u_i}{\partial x_j} g_i g_j \right\rangle = -\frac{2}{\mathrm{Pe}^2} \sum_i \langle |\nabla g_i|^2 \rangle \tag{15}$$

Alternatively, in direct tensorial notation,

$$\frac{d\epsilon}{dt} + \frac{2}{\mathrm{Pe}} \langle \nabla \boldsymbol{u} : \boldsymbol{g} \otimes \boldsymbol{g} \rangle = -\frac{2}{\mathrm{Pe}^2} \langle \nabla \boldsymbol{g} : \nabla \boldsymbol{g} \rangle, \tag{16}$$

where $\otimes$ denotes a dyadic product of two vectors resulting in a second-order tensor, and : denotes double contraction.

Equations (11) and (16) are *exact* evolution equations for the global concentration variance σ^2 and the mean scalar dissipation rate ϵ, respectively. Clearly, closure relations are needed for this system of equations to be solvable, and the objective of this paper is precisely to propose a closure model, guided by direct numerical simulation of the underlying partial differential equations. The form of Eq. (16), however, already reveals that the heart of the problem lies in the interplay between velocity gradients (flow disorder) and concentration

gradients. Since gradients in concentration lead to contrasts in fluid viscosity, homogenization of the mixture through removal of the concentration gradients also results in destruction of the viscosity contrasts, that is, decay of viscous fingering. Equation (11) reflects that the degree of mixing increases monotonically in time. One could naively expect, in view of the right-hand side of Eq. (16), that the same be true for the scalar dissipation rate. However, this is not the case: as we shall see, concentration gradients increase during the early stages of viscous fingering before starting to decrease, resulting in a nontrivial behavior for the scalar dissipation rate and the overall mixing process.

III. NUMERICAL METHOD

A. Stream function-vorticity method

The pressure equation (5), is an elliptic PDE with a space- and time-varying coefficient. Solving this equation is computationally expensive for a large number of grid cells, which is required to resolve the concentration gradients that ensue as a result of the viscous instability at high Pe. To alleviate this computational burden, the governing equations are usually cast in the so-called stream function-vorticity (SV) formulation, and the "pressure" equation solved using a spectral method [30,32,55].

The stream function Ψ is defined for an incompressible two-dimensional velocity field as

$$u_x = \frac{\partial \Psi}{\partial y}, \quad u_y = -\frac{\partial \Psi}{\partial x}. \tag{17}$$

The magnitude of the vorticity vector normal to the plane of flow, $\omega \equiv |\nabla \times \boldsymbol{u}|$, is related to the gradients in concentration field. Using the definition of the Darcy velocity Eq. (4) and the exponential form of the mixture viscosity,

$$\omega = R\,|\nabla c \times \boldsymbol{u}| = R\left(\frac{\partial c}{\partial x}u_y - \frac{\partial c}{\partial y}u_x\right). \tag{18}$$

Using the definitions of the stream function and vorticity, we obtain the relation

$$\nabla^2 \Psi = -\omega. \tag{19}$$

In the stream function-vorticity method, Eqs. (3) and (19) are solved sequentially under periodic boundary conditions. At a given time step, Eq. (18) is used to compute the vorticity field from known concentration and velocity fields. Then Eq. (19), which is a single algebraic equation in Fourier space under periodic boundary conditions, is solved to obtain the stream function of the flow at the next time step using the vorticity at previous time step. The velocity field is then constructed from the stream function using Eq. (17).

This computational approach has been used successfully for the nonlinear simulation of the viscous fingering phenomenon [30,32,55], with a degree of fidelity and resolution that was not possible in early simulations [29,31]. However, this formulation is numerically unstable and fails to produce a solution for large values of mobility ratio ($M > 20$ or $R > 3$), when the fingertip velocity is much higher than the mean flow velocity. The underlying reason for the numerical instability is the mobility splitting inherent to Eq. (19), which computes the stream function at the current time step from the vorticity at the previous time step. This split is stable for moderate values of M but becomes unconditionally unstable for large values of M, irrespective of time-step size.

B. Implicit mobility method

Obtaining a numerical scheme that is stable at high M requires an implicit mobility scheme. To this end, we solve Eq. (5) globally for the pressure field. This is computationally more expensive because it entails building and solving a linear system of equations at each time step, instead of one single equation in Fourier space Eq. (19). However, since the solution of Eq. (5) implies implicitness—the velocity at a time step corresponds to the mobility at the same time step—this scheme is stable for arbitrarily high values of M. We use a finite-volume method with two-point flux approximation (TPFA) to discretize the Darcy flux between the grid cells [76]. We solve the linear system of equations resulting from discretizating Eq. (5) using either a direct solver or an iterative multigrid solver. The concentration equation is solved using a sixth-order compact finite differences and a third-order Runge-Kutta time-stepping scheme [45].

We use a finite-volume discretization of the divergence-free velocity condition in Eq. (3). Integrating over the volume of the ith cell V^i and using the divergence theorem

$$\int_{V^i} \nabla \cdot \boldsymbol{u} = \int_{S^i} \boldsymbol{u} \cdot \boldsymbol{n} dS = 0, \tag{20}$$

where S^i is the total surface area of the cell, composed of interfaces S^{ij}, where j denotes cells adjacent to the ith cell. Thus, fluid mass balance over cell i for an incompressible flow becomes

$$\sum_j U^{ij}(t) = 0, \tag{21}$$

where U^{ij} is the integrated flux through interface S^{ij}. The pressure field $p(x,y)$ is approximated as a piecewise constant function, taking discrete values p^i at individual cells. Fluxes across interfaces are estimated from a set of neighboring cell pressures. The TPFA method uses just two neighboring cell pressures, p^i and p^j, to approximate the flux through the interface ij,

$$U^{ij} = t^{ij}\lambda^{ij}(p^i - p^j), \tag{22}$$

where λ^{ij} is the mobility at the ij-interface, estimated by a harmonic average of the respective cell mobilities, $1/\mu^i$ and $1/\mu^j$, and t^{ij} is the interface geometric transmissibility, which for a regular 2D Cartesian grid is proportional to the length of the interface and inversely proportional to the distance between cell centers. Thus, the interface transmissibility $T^{ij} = t^{ij}\lambda^{ij}$ is, for a simple 2D Cartesian grid,

$$T_x^{ij} = \frac{h_y}{h_x}\frac{2}{\mu^i + \mu^j}, \quad T_y^{ij} = \frac{h_x}{h_y}\frac{2}{\mu^i + \mu^j}, \tag{23}$$

for vertical and horizontal interfaces, respectively.

Equations (21) and (22) result in a system of linear equations to be built and solved at every time step,

$$\boldsymbol{T}\,\boldsymbol{P} = \boldsymbol{B}, \tag{24}$$

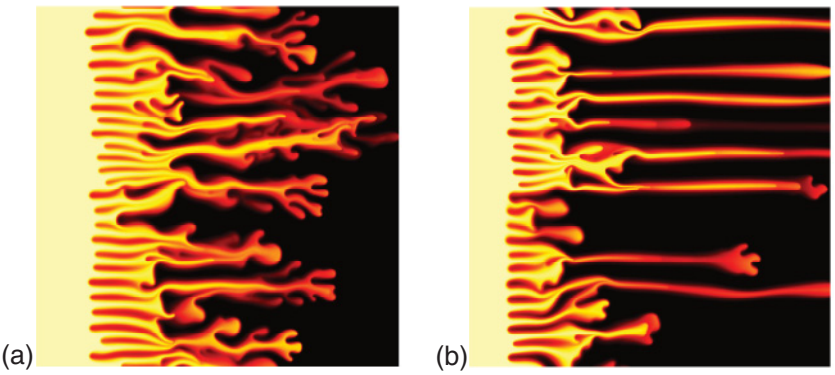

FIG. 1. (Color online) Snapshots of the concentration field from viscous fingering simulations using the implicit mobility TPFA method. (a) $R = 4$, $\mathrm{Pe} = 5000$. (b) $R = 5$, $\mathrm{Pe} = 5000$. Channeling of the fingers of less viscous fluid at high R renders the explicit mobility stream function-vorticity method unstable.

where $\boldsymbol{P}$ is the vector of unknown cell-center pressures and $\boldsymbol{B}$ is the vector of known boundary fluxes. Generation and assembly of the mobility-dependent transmissibility matrix, $\boldsymbol{T}$, for the simple periodic boundary conditions as considered here, can be completely vectorized.

IV. NONLINEAR SIMULATIONS

A. Continuous injection

To illustrate the ability of the implicit high-resolution numerical method to simulate viscous fingering for high viscosity ratios, we solve the governing equations on a square domain with periodic boundary conditions in the y direction and uniform flux on the left and right boundaries. Initially, the medium is filled with the more viscous fluid, and the less viscous fluid is injected through the left boundary. For high viscosity ratios ($R = 4$, corresponding to $M \approx 55$), the invading fluid fingers through the defending fluid aggressively [Fig. 1(a)], exhibiting well-known complex nonlinear interactions such as finger merging, shielding, and tip splitting [30,32]. Simulation of the flow for this viscosity contrast is outside the range of stability of the stream function-vorticity method. For an even larger viscosity ratio ($R = 5$, corresponding to $M \approx 150$), a new pattern emerges: *channeling* through the more viscous fluid, with minimal interaction between channels and very low sweep efficiency [Fig. 1(b)].

B. Mixing of randomized blobs

To understand the effect of viscous fingering on fluid mixing we numerically solve the governing equations (3) and (4), on a square domain with periodic boundary conditions. The periodic boundary conditions allow us to focus on the dissipative nature of viscous fingering in absence of any boundary effects.

We investigate a scenario in which the two fluids are segregated as a set of randomly shaped blobs of the more viscous fluid surrounded by the connected, less viscous fluid (Fig. 2). Each fluid occupies 50% of the volume and, since the boundary conditions are biperiodic, $\langle c \rangle \equiv 0.5$ throughout the entire simulation. The characteristic diameter of the initial blobs is about one-sixth of the length of the domain, and the system evolves under an imposed gradient from left to right. If both fluids had the same viscosity, the blobs would simply translate in the x direction and slowly diffuse into the ambient fluid. The situation is radically different in the presence of a viscosity contrast. Onset of fingering driven by advection creates new interfacial area through stretching and splitting of the initial interface around the blobs, thereby enhancing diffusive mixing because both the interfacial area and the concentration gradients are larger. This is quantitatively reflected in the nonmonotonic time evolution of the scalar dissipation rate, which achieves a maximum precisely as a result of fingering-induced mixing (Fig. 3). At later times, the strength of the instability decays due to homogenization of the mixture and, asymptotically, mixing is again controlled by diffusion.

To illustrate that mixing under viscous fingering is strongly dependent on the flow conditions, we simulate the scenario in which blobs of less viscous fluid are transported and dispersed through a more viscous ambient fluid. Viscous fingers now emerge out of the blobs and into the connected fluid. The initial

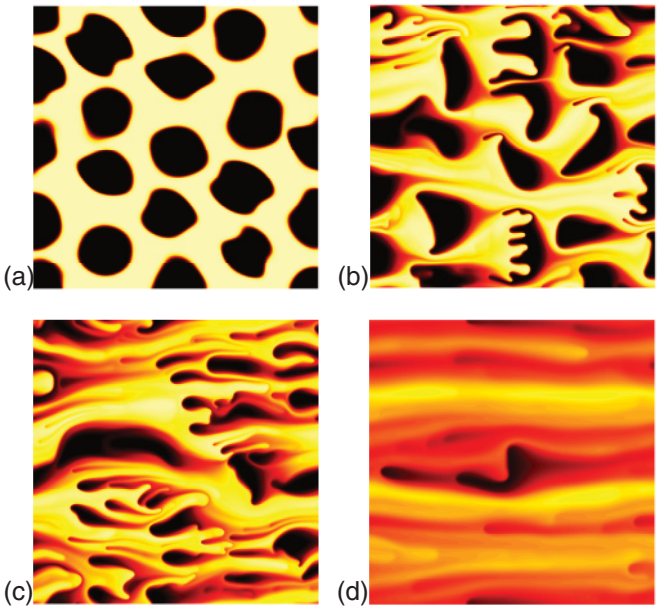

FIG. 2. (Color online) Snapshots of the concentration field at increasing time steps from a numerical simulation of miscible viscous fingering. A set of more viscous blobs (dark) is displaced through a less viscous fluid (light) under left-to-right flow and periodic boundary conditions. Fingers of the less viscous fluid initiate at the unstable interface, grow inside the more viscous blobs, split into multiple fingers, coalesce together, and connect across the blobs as the two fluids mix. The displacement corresponds to a viscosity ratio $M = \exp(2) \approx 7$ and Péclet number $\mathrm{Pe} = 10^4$.

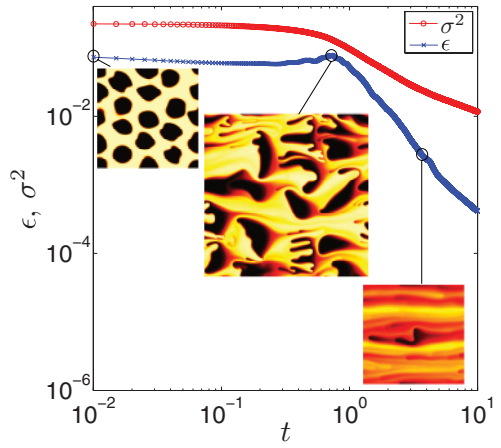

FIG. 3. (Color online) Evolution of mean scalar dissipation rate (blue crosses) and concentration variance (red circles) for a flow scenario in which blobs of more viscous fluid are displaced through a less viscous fluid. The mixing rate increases and reaches a maximum at early times due to the flow disorder induced by viscous fingering. The displacement corresponds to a viscosity ratio $M = \exp(2) \approx 7$ and Péclet number $\mathrm{Pe} = 10^4$.

interfacial area available for the initiation and growth of the fingers is larger in this case than in the previous configuration (blobs of more viscous fluid). Moreover, the less viscous fluid must initially penetrate through the more viscous fluid before it forms a connected "phase." As a result of the earlier finger initiation and more aggressive tip splitting, the scalar dissipation rate ϵ exhibits a larger and earlier hump in the scalar dissipation rate (Fig. 4), which translates into faster mixing.

V. MIXING MODEL

We are interested in developing an upscaled model of the mixing process that incorporates the details of the viscous fingering phenomenon. Thus, the objective is to obtain mixing model in terms of evolution equations for the global variables, σ^2 and ϵ, that incorporates the correct dependency on the physical parameters, R and Pe.

To arrive at such a macroscopic description, we must model the "advective" and "diffusive" terms in the exact equation for the mean scalar dissipation rate, Eq. (16). The advective term involves the interaction between velocity gradients and concentration gradients. As we will see, dealing with the gradient of velocity field requires modeling of the interface stretching associated with tip-splitting and channeling events. As an intermediate step toward modeling the advective term, we present a model for mean mechanical dissipation rate, ϵ_u. The diffusive term in Eq. (16) is responsible for the removal of the fluid interfaces either resulting from the splitting and channeling events or being present as part of the initial configuration (e.g., blob interfaces).

A. Mechanical dissipation rate

The mean mechanical dissipation rate is defined as

$$\epsilon_u = 2\langle \nu \nabla^{\mathrm{s}} \boldsymbol{u} : \nabla^{\mathrm{s}} \boldsymbol{u} \rangle, \tag{25}$$

where ν is the kinematic viscosity of the mixture, and superscript s denotes symmetric part of the tensor. Hence, $\nabla^{\mathrm{s}} \boldsymbol{u}$ is the rate-of-strain tensor, responsible for interface stretching.

From Darcy's equation (4), we have

$$\nabla \boldsymbol{u} = -\mu^{-1}[R \nabla c \otimes \nabla p + \nabla (\nabla p)]. \tag{26}$$

In a viscous fingering process, $R \nabla c \otimes \nabla p$ and $\nabla(-\nabla p)$ terms evolve similarly in time (Fig. 5). Thus, we propose the scaling

$$\nabla \boldsymbol{u} \sim -\mu^{-1}[R \nabla c \otimes \nabla p] \sim R \boldsymbol{u} \otimes \boldsymbol{g}. \tag{27}$$

Therefore, assuming a spatially averaged kinematic viscosity $\langle \nu \rangle$, ϵ_u can be approximated as

$$\begin{aligned} \epsilon_u &\sim 2\langle \nu \rangle R^2 \langle \mu^{-2} |(\nabla c \otimes \nabla p)^{\mathrm{s}}|^2 \rangle \\ &\sim 2\langle \nu \rangle R^2 \langle |(\boldsymbol{u} \otimes \boldsymbol{g})^{\mathrm{s}}|^2 \rangle. \end{aligned} \tag{28}$$

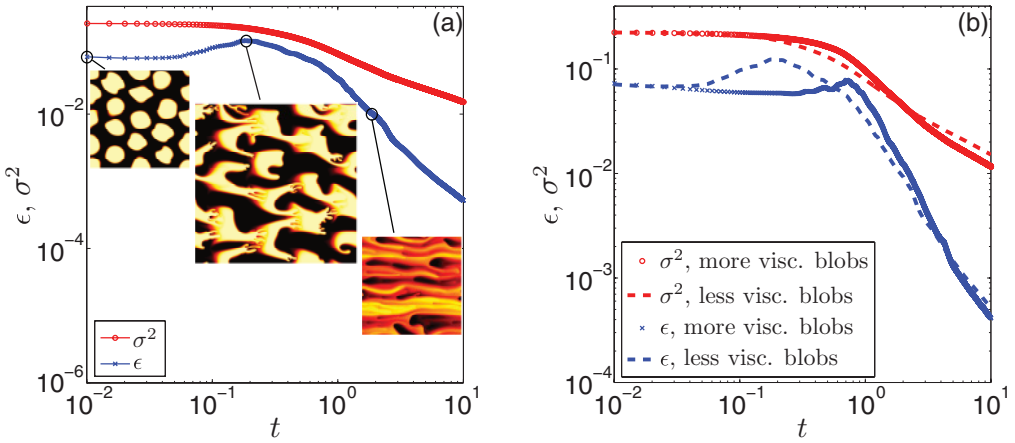

FIG. 4. (Color online) (a) Evolution of mean scalar dissipation rate (blue crosses) and concentration variance (red circles) for blobs of less viscous fluid in a more viscous medium. (b) Comparison of the two scenarios, when the initial blobs are either more viscous or less viscous than the ambient fluid. The case with less viscous blobs leads to earlier and larger hump in the evolution of the scalar dissipation rate ϵ. This results in faster decay of the concentration variance at early times. The simulations correspond to $R = 2$, $\mathrm{Pe} = 10^4$.

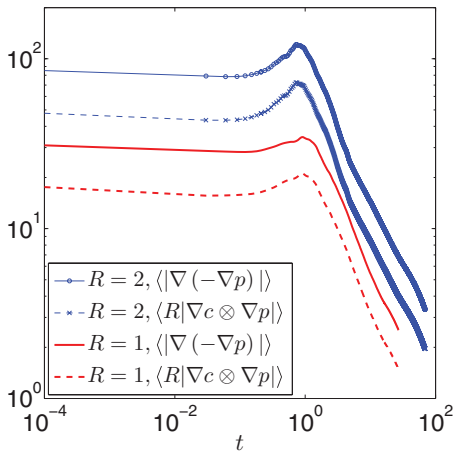

FIG. 5. (Color online) Evolution in time of the terms $\langle R|\nabla c \otimes \nabla p|\rangle$ (dashed line) and $\langle|\nabla(-\nabla p)|\rangle$ (solid line) from direct numerical simulations for $\mathrm{Pe} = 10^4$ and two different values of R: $R = 1$ (red) and $R = 2$ (blue). For each value of R, the time evolution of both terms is very similar.

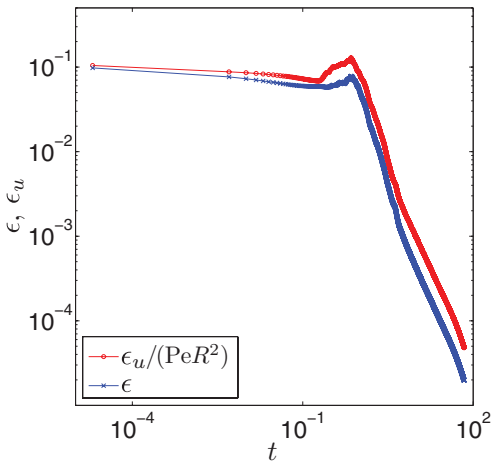

FIG. 6. (Color online) Evolution of ϵ (blue crosses) and $\epsilon_u/(\mathrm{Pe}R^2)$ (red circles) from direct numerical simulation, for $R = 2$ and $\mathrm{Pe} = 10^4$. The two variables evolve similarly, confirming the proposed scaling in Eq. (32).

Using the Frobenius norm of a tensor,

$$|(\boldsymbol{u} \otimes \boldsymbol{g})^s|^2 = \tfrac{1}{2}[|\boldsymbol{u}|^2|\boldsymbol{g}|^2 + (\boldsymbol{u} \cdot \boldsymbol{g})^2]. \tag{29}$$

Hence,

$$\epsilon_u \sim \langle \nu \rangle R^2 \langle |\boldsymbol{u}|^2 |\boldsymbol{g}|^2 (1 + \cos^2\theta) \rangle, \tag{30}$$

where θ is the angle between vectors $\boldsymbol{u}$ and $\boldsymbol{g}$ at the interface. Assuming homogeneity of the viscous fingering process, we can split the average of the product as product of the averages (as in the case of statistically homogeneous turbulence [77]). Neglecting the $\cos^2\theta$ term, which is small compared to the other term,

$$\epsilon_u \sim \langle \nu \rangle R^2 \langle |\boldsymbol{g}|^2 \rangle \langle |\boldsymbol{u}|^2 \rangle. \tag{31}$$

Taking the mean flow speed U as constant and using $\epsilon \equiv \langle |\boldsymbol{g}|^2 \rangle / \mathrm{Pe}$, we obtain

$$\epsilon_u \sim R^2 \mathrm{Pe} \epsilon. \tag{32}$$

We have verified this relationship between the scalar and mechanical mean dissipation rates by means of direct numerical simulation (Fig. 6).

B. Scalar dissipation rate

From Eq. (27), we approximate the advective term in Eq. (16) as

$$\frac{2}{\mathrm{Pe}} \langle \nabla \boldsymbol{u} : \boldsymbol{g} \otimes \boldsymbol{g} \rangle \sim \frac{2}{\mathrm{Pe}} \langle R |\boldsymbol{g}|^2 (\boldsymbol{u} \cdot \boldsymbol{g}) \rangle. \tag{33}$$

Assuming, as before, statistical homogeneity at high Pe,

$$\begin{aligned} \frac{2}{\mathrm{Pe}} \langle R |\boldsymbol{g}|^2 (\boldsymbol{u} \cdot \boldsymbol{g}) \rangle &\sim -\frac{2R}{\mathrm{Pe}} \langle |\boldsymbol{g}|^3 \rangle \langle |\boldsymbol{u}| \rangle \langle \cos\theta \rangle \\ &\sim -2R\sqrt{\mathrm{Pe}} \langle \cos\theta \rangle \epsilon^{3/2}, \end{aligned} \tag{34}$$

where we used the definition of ϵ. We take $\langle \cos\theta \rangle = e^{-R/4} \epsilon / \sigma^2$, a model that agrees well with the simulations (Fig. 7). The effect of channeling at higher viscosity contrasts is to reduce $\langle |\boldsymbol{g}| \rangle$ (by reducing the total interfacial area) and realign the concentration gradient vector to become orthogonal to the velocity vector. Hence,

$$\frac{2}{\mathrm{Pe}} \langle \nabla \boldsymbol{u} : \boldsymbol{g} \otimes \boldsymbol{g} \rangle \sim -2R\sqrt{\mathrm{Pe}}\, e^{-R/4} \frac{\epsilon^{5/2}}{\sigma^2}. \tag{35}$$

Now, we model the diffusive term in Eq. (16),

$$\frac{2}{\mathrm{Pe}^2} \langle \nabla \boldsymbol{g} : \nabla \boldsymbol{g} \rangle = \frac{2}{\mathrm{Pe}^2} \langle |\nabla \boldsymbol{g}|^2 \rangle = \frac{2}{\mathrm{Pe}^2} \frac{\langle |\nabla \boldsymbol{g}|^2 \rangle}{\mathrm{var}(\boldsymbol{g})} \mathrm{var}(\boldsymbol{g}), \tag{36}$$

where $\mathrm{var}(\boldsymbol{g}) = \langle |\boldsymbol{g}|^2 \rangle - \langle |\boldsymbol{g}| \rangle^2$. Under the assumption of a unique characteristic transverse length scale in the problem,

$$\frac{\langle g_i^2 \rangle}{\langle |\nabla g_i|^2 \rangle} \sim \frac{\langle c^2 \rangle}{\langle |\nabla c|^2 \rangle}, \quad \frac{\langle g_i \rangle}{\langle |\nabla g_i|^2 \rangle} \sim \frac{\langle c \rangle}{\langle |\nabla c|^2 \rangle}. \tag{37}$$

Therefore, using the definition of the dissipation length scale s, we can write,

$$\frac{\mathrm{var}(g_i)}{\langle |\nabla g_i|^2 \rangle} \sim \frac{\mathrm{var}(c)}{\langle |\nabla c|^2 \rangle} = s^2 \tag{38}$$

For the diffusive term, this means,

$$\frac{2}{\mathrm{Pe}^2} \langle \nabla \boldsymbol{g} : \nabla \boldsymbol{g} \rangle \sim \frac{2}{\mathrm{Pe}^2} \frac{\langle |\nabla c|^2 \rangle}{\mathrm{var}(c)} \mathrm{var}(\boldsymbol{g}) = \frac{2}{\mathrm{Pe}} \frac{\epsilon}{\sigma^2} \mathrm{var}(\boldsymbol{g}). \tag{39}$$

If we can assume that $\langle |\boldsymbol{g}|^2 \rangle \sim \langle |\boldsymbol{g}| \rangle^2$, then $\mathrm{var}(\boldsymbol{g}) \sim \langle |\boldsymbol{g}|^2 \rangle = \epsilon \mathrm{Pe}$, which leads to

$$\frac{2}{\mathrm{Pe}^2} \langle \nabla \boldsymbol{g} : \nabla \boldsymbol{g} \rangle \sim 2 \frac{\epsilon^2}{\sigma^2}. \tag{40}$$

This scaling for diffusive decay of ϵ provides insight into the relation among $d\epsilon/dt$, ϵ, and σ^2: the rate of decay of the mean dissipation rate due to diffusion follows the nonmonotonicity in ϵ, with its strength scaled by the variance, which is monotonic in time. Using this insight, we can further improve the model for the diffusive term. Using the ADE,

$$\begin{aligned} \frac{2}{\mathrm{Pe}^2} \langle \nabla \boldsymbol{g} : \nabla \boldsymbol{g} \rangle &\sim 2 \langle (\partial_t c + \boldsymbol{u} \cdot \boldsymbol{g})^2 \rangle \\ &\sim 2 \langle (\partial_t c)^2 + \partial_t c (\boldsymbol{u} \cdot \boldsymbol{g}) \rangle. \end{aligned} \tag{41}$$

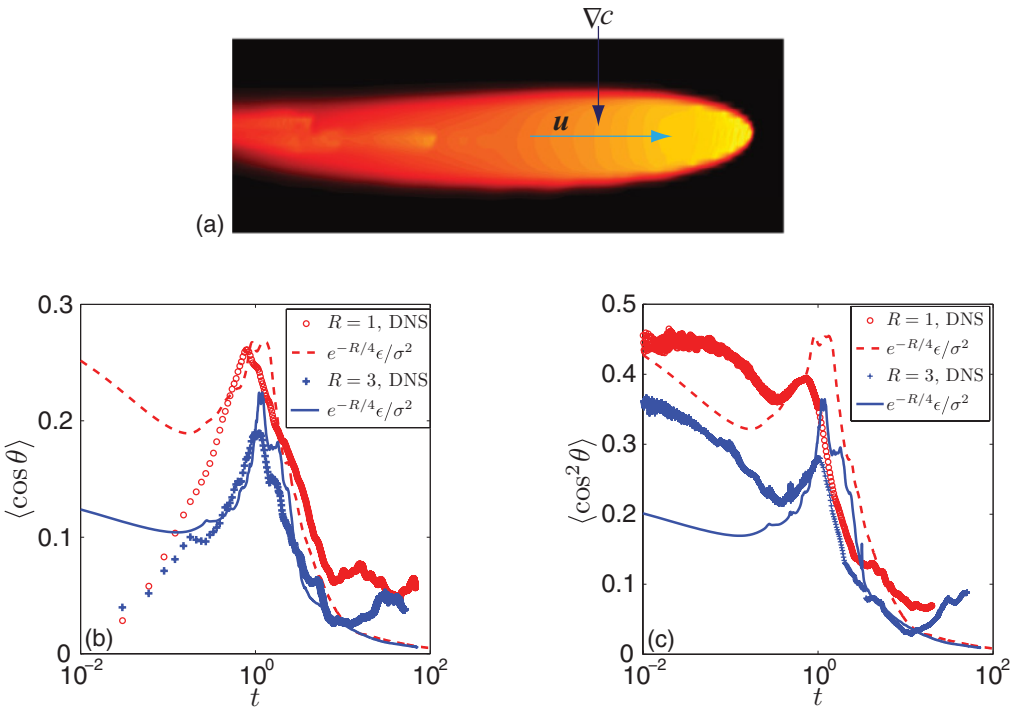

FIG. 7. (Color online) Effect of channeling on the evolution of $\langle\cos\theta\rangle$ and $\langle\cos^2\theta\rangle$. (a) Channeling of the less viscous fluid at high R means that vectors $\boldsymbol{u}$ and ∇c are approximately orthogonal ($\theta \approx \pi/2$) along the body of the channel except near the tip. This reduces $\langle\cos\theta\rangle$ because channels dominate the flow (suppress tip-splitting) in the entire domain. Comparison of the time evolution of $\langle\cos\theta\rangle$ (b) and $\langle\cos^2\theta\rangle$ (c) from the direct numerical simulations and the proposed model $\langle\cos\theta\rangle = e^{-R/4}\epsilon/\sigma^2$, for $R = 1,3$ and $\mathrm{Pe} = 10^4$.

We model $\langle(\partial_t c)^2\rangle \sim \frac{1}{\sigma^2}(\frac{d\sigma^2}{dt})^2 \sim \frac{\epsilon^2}{\sigma^2}$ and $-\langle\partial_t c(\boldsymbol{u}\cdot\boldsymbol{g})\rangle \sim \langle(\boldsymbol{u}\cdot\boldsymbol{g})^2\rangle \sim \mathrm{Pe}\epsilon\langle\cos^2\theta\rangle$. From Fig. 7 and the scaling of the diffusive term with ϵ and σ^2 found through numerical simulation, we obtain

$$\frac{2}{\mathrm{Pe}^2}\langle\nabla\boldsymbol{g} : \nabla\boldsymbol{g}\rangle \sim \sqrt{R\mathrm{Pe}\, e^{-R/4}}\left(\frac{\epsilon}{\sigma}\right)^{5/2}. \tag{42}$$

Using Eqs. (35) and (42), the model equation for ϵ under viscous fingering ($R > 0$) becomes

$$\frac{d\epsilon}{dt} - AR\sqrt{\mathrm{Pe}}\, e^{-R/4}\frac{\epsilon^{5/2}}{\sigma^2} + B\sqrt{R\mathrm{Pe}\, e^{-R/4}}\left(\frac{\epsilon}{\sigma}\right)^{5/2} = 0, \tag{43}$$

where A and B are two model parameters. Equation (43) has two terms corresponding to fingering-induced enhancement and diffusion-driven decrease in the dissipation rate. The advection-driven term is negative and gives the rising behavior in ϵ, whereas the diffusion-driven term is positive and gives the declining behavior in ϵ.

Equations (11) and (43) form a coupled system of first-order ODEs which can be solved with initial values of σ^2 and ϵ. We test the performance of the mixing model by comparing the predicted decay of variance and scalar dissipation rate with results from the direct numerical simulations (Fig. 8).

VI. EFFECTIVE AVERAGE VISCOSITY

As a result of the exponential dependence of fluid viscosity on solvent concentration, the average (effective) viscosity in the flow domain decreases as the less viscous fluid starts to mix with the more viscous one. The rate of decrease is faster at early times and slower at later times, giving rise to an inflection point in the evolution of the average viscosity. Since the rate of change in viscosity is linked to changes in interface length resulting from fingering, we hypothesize that ϵ and $d\overline{\mu}/dt$ are intimately related. Here, we present a relationship between the mean scalar dissipation rate, ϵ, and the domain average viscosity, $\overline{\mu}$.

The average mixture viscosity $\overline{\mu}$ can be expressed as

$$\overline{\mu} = \frac{1}{A_t}\int_0^1 \mu dA, \tag{44}$$

where dA is the area enclosed by contours $c = c^* + \delta c^*$ and $c = c^*$, and μ is the mixture viscosity inside dA, and $A_t = 1$ is the total area of the domain. The area (mass) occupied by the fluid in regions where $c \leqslant c^*$ at a given time t is also the area enclosed by concentration isosurface $c = c^*$, and is defined as

$$A(c^*,t) \equiv \int_{c\leqslant c^*} dS. \tag{45}$$

Since the A-c and A-μ relations are one-to-one at any given time (Fig. 9), we can replace the integral in A with an equivalent integral in μ,

$$\overline{\mu} = \frac{1}{A_t}\int_1^{e^R} A d\mu. \tag{46}$$

Differentiating with respect to time,

$$\frac{d\overline{\mu}}{dt} = \frac{1}{A_t}\int_1^{e^R}\frac{\partial A}{\partial t}d\mu. \tag{47}$$

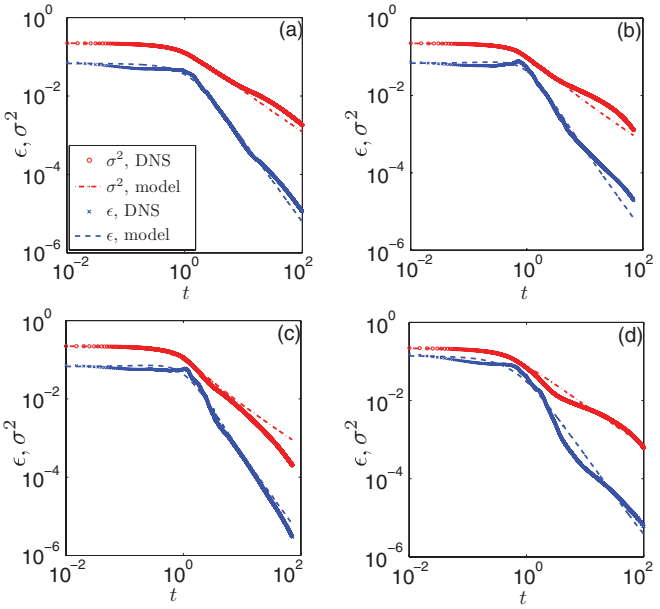

FIG. 8. (Color online) Performance of the mixing model given by Eqs. (11) and (43). Comparison of the evolution of ϵ (blue) and σ^2 (red) in the simulation (symbols) and the proposed model (dashed line) for different values of R and Pe. (a), $R = 1$, $\mathrm{Pe} = 10^4$. (b), $R = 2$, $\mathrm{Pe} = 10^4$. (c), $R = 3$, $\mathrm{Pe} = 10^4$. (d), $R = 3$, $\mathrm{Pe} = 10^3$. The same values of the two model parameters were used for all cases: $A = 0.76$, $B = 0.84$.

Using the the divergence-free velocity condition and the identity [78]

$$\oint_{c=c^*} \frac{(\cdot)}{|\nabla c|} dl = \frac{\partial}{\partial c^*} \int_{c \leqslant c^*} (\cdot)\, dS, \tag{48}$$

where the circuit integral is defined on the concentration contour $c = c^*$, we obtain

$$\frac{\partial}{\partial t} A(c^*,t) = -\frac{1}{\mathrm{Pe}} \frac{\partial}{\partial c^*} \int_{c \leqslant c^*} \nabla^2 c\, dS, \tag{49}$$

which is a statement that the contour area changes only due to diffusive flux (from fluid in $c > c^*$ area to the fluid in $c < c^*$ area) as pure advection conserves the contour area. Using Eq. (48), the right-hand-side term in Eq. (49) can be written as

$$\int_{c \leqslant c^*} \nabla^2 c\, dS = \oint_{c=c^*} \nabla c \cdot \boldsymbol{n} dl = \oint_{c=c^*} \nabla c \cdot \frac{\nabla c}{|\nabla c|} dl = \frac{\partial}{\partial c^*} \int_{c \leqslant c^*} |\nabla c|^2 dS. \tag{50}$$

Hence, Eq. (49) can be transformed into

$$\frac{\partial}{\partial t} A(c^*,t) = -\frac{1}{\mathrm{Pe}} \frac{\partial}{\partial c^*} \left(\langle |\nabla c|^2 \rangle_{c^*} \frac{\partial A}{\partial c^*} \right), \tag{51}$$

where the average of a field on the tracer contour $c = c^*$ is defined as

$$\langle \cdot \rangle_{c^*} \equiv \frac{\partial}{\partial A} \int_{c \leqslant c^*} (\cdot)\, dS. \tag{52}$$

Equation (51) can be expressed in terms of the mean dissipation rate,

$$\frac{\partial A}{\partial t} = -\frac{\partial}{\partial c^*} \left(\epsilon^* \frac{\partial A}{\partial c^*} \right), \tag{53}$$

where $\epsilon^* = \frac{1}{\mathrm{Pe}} \langle |\nabla c|^2 \rangle_{c^*}$ is the conditional mean dissipation rate of scalar variance for $c = c^*$. Integrating ϵ^* with respect to A,

$$\int_0^1 \epsilon^* dA = \frac{1}{\mathrm{Pe}} \int_{c^*=0}^{c^*=1} d \left(\int_{c \leqslant c^*} |\nabla c|^2 dS \right) = \frac{1}{\mathrm{Pe}} \left[\int_{c \leqslant c^*} |\nabla c|^2 dS \right]_{c^*=0}^{c^*=1} = \frac{1}{\mathrm{Pe}} \int |\nabla c|^2 dS = A_t \epsilon, \tag{54}$$

and using Eq. (53), we obtain

$$\frac{d\overline{\mu}}{dt} = -\frac{1}{A_t} \int_1^{e^R} \frac{\partial}{\partial c^*} \left(\epsilon^* \frac{\partial A}{\partial c^*} \right) d\mu. \tag{55}$$

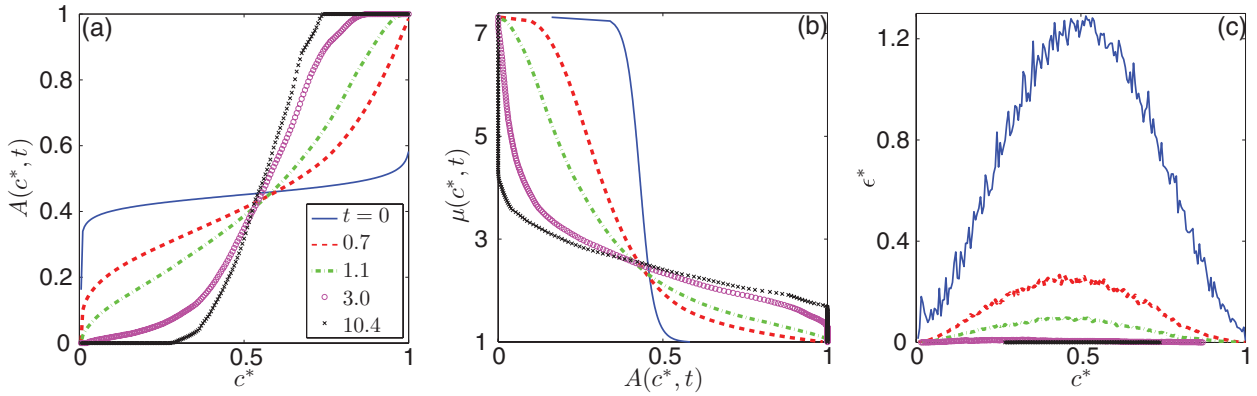

FIG. 9. (Color online) Evolution of the variables $A(c^*)$, $\mu(c^*)$ and ϵ^* during the simulation of mixing of blobs of more viscous fluid with $R = 2$, $\mathrm{Pe} = 10^4$ (Fig. 2). (a) Plot of $A(c^*,t)$, the area of the domain enclosed by the contour of $c = c^*$, that is, satisfying the inequality $c \leqslant c^*$ [Eq. (45)]. It is a monotonically increasing function of c^* that evolves in time due to mixing from a perfectly segregated state to a fully homogenized mixture. (b) Relation between the average viscosity $\mu(c^*)$ and contour area $A(c^*)$, which is a one-to-one relation at all times. High values of viscosity, in the range $\sim e^R$, are quickly suppressed due to mixing. (c) Plot of the conditional mean dissipation rate ϵ^* as a function of the contour concentration c^*, which satisfies that $\epsilon^* = 0$ at both $c^* = 0$ and $c^* = 1$.

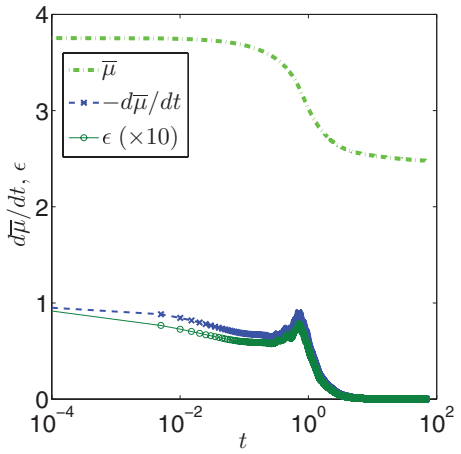

FIG. 10. (Color online) Relationship between the rate of decrease in average viscosity $\overline{\mu}$ (green dashed line) and the mean scalar dissipation rate ϵ (green circles) [Eq. (58)]. The inflection point in the average viscosity curve, which corresponds to a minimum in the $d\overline{\mu}/dt$ (blue crosses), occurs at the same time as ϵ reaches its maximum. The numerical simulations correspond to $R = 2$ and $\mathrm{Pe} = 10^4$.

For our viscosity model $\mu(c) = e^{R(1-c)}$, $d\mu = -R\mu dc$, so

$$\frac{d\overline{\mu}}{dt} = \frac{R}{A_t}\int_1^0 \mu \frac{\partial}{\partial c^*}\left(\epsilon^* \frac{\partial A}{\partial c^*}\right) dc = -\frac{R}{A_t}\int_{c^*=0}^{c^*=1} \mu d\left(\epsilon^* \frac{\partial A}{\partial c^*}\right). \tag{56}$$

Since $\epsilon^* = 0$ at $c^* = 0$ and $c^* = 1$ (Fig. 9),

$$\frac{d\overline{\mu}}{dt} = -\frac{R}{A_t}\left[\left(\mu\epsilon^* \frac{\partial A}{\partial c^*}\right)_{\epsilon^*=0}^{\epsilon^*=0} - \int_{e^R}^1 \epsilon^* \frac{\partial A}{\partial c^*} d\mu\right] = -\frac{R}{A_t}\int_0^1 \epsilon^* \frac{\partial A}{\partial c^*} R\mu dc = -\frac{R^2}{A_t}\int_0^1 \mu\epsilon^* dA \sim -\frac{R^2\overline{\mu}}{A_t}\int_0^1 \epsilon^* dA. \tag{57}$$

Finally, using Eqs. (54) in Eq. (47), we obtain the desired relation:

$$\frac{d\overline{\mu}}{dt} \sim -R^2\overline{\mu}\epsilon, \tag{58}$$

or, equivalently,

$$\frac{d\log\overline{\mu}}{dt} \sim -R^2\epsilon. \tag{59}$$

Thus, our analysis suggests that the rate of decrease in mixture viscosity is directly proportional to the mean dissipation rate and that, as a result, a maximum ϵ corresponds to a maximum (with negative sign) in $d\overline{\mu}/dt$. This result, which is confirmed by direct numerical simulations (Fig. 10), could allow the determination of ϵ in a laboratory experiment, where average viscosity is being measured at discrete time intervals.

VII. DISCUSSION AND CONCLUSIONS

Viscous fingering acts as an agent for enhanced mixing by creating additional interfacial area and disorder in the flow field. The rate of mixing quantified through the mean scalar dissipation rate, ϵ, increases at early times as additional interface is created through finger stretching and tip-splitting.

The impact of the viscous instability on mixing, however, is nontrivial. For moderate viscosity contrasts (roughly $M < 10$, or $R < 2.5$), larger M implies a larger increase in ϵ due to fingering, and, therefore, faster mixing. However, as M is increased beyond a value of 10, channeling of the less viscous fluid starts to dominate the flow, leading to flow focusing across the entire flow domain and inhibiting the growth of adjacent fingers. As a result of this channeling phenomenon, which slows down the creation of additional interface area, growth in ϵ is not only delayed but also limited in the magnitude (Fig. 11). Hence, in this regime of very large viscosity contrast, mixing is less efficient. Fastest mixing is achieved at an optimum viscosity ratio that maximizes the creation of fluid-fluid interfacial area across which diffusive mixing takes place. Channeling and tip-splitting

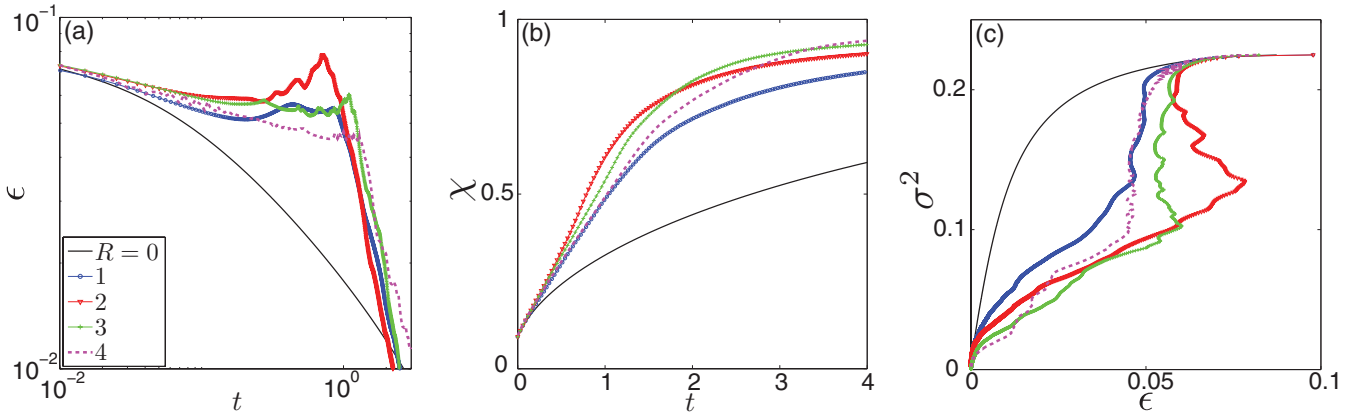

FIG. 11. (Color online) (a) Evolution of the mean scalar dissipation rate ϵ. (b) Evolution of the degree of mixing $\chi = 1 - 4\sigma^2$. (c) Crossplot of $\sigma^2 - \epsilon$, for different values of the viscosity ratio, and $\mathrm{Pe} = 10^4$. The largest hump in dissipation rate, which leads to fastest initial mixing, occurs for $R \sim 2.5$.

play an important role in this balancing act, which makes degree of mixing a nonmonotonic function of the viscosity contrast.

In this article, we presented an upscaled model of fingering-driven mixing under the assumption of statistical homogeneity. The model captures the characteristic stretching of the material interface over which diffusive mixing takes place. It takes the form of two coupled ODEs to be solved for the concentration variance and mean dissipation rate. At the heart of the model, which is inspired by turbulence modeling, is the recognition that the properties of the velocity field (through modeling of the mechanical dissipation rate) are essential in the homogenization of concentration gradients. We guided and validated the model by means of direct numerical simulations of miscible viscous fingering over a large range of viscosity ratios and Péclet numbers. For values of the viscosity ratio larger than 20, the traditional (and very efficient) stream function-vorticity formulation is numerically unstable. We used a high-resolution implicit mobility numerical method that, while being computationally more expensive, guarantees stability and allowed us to obtain fully resolved simulations of the fingering phenomenon.

ACKNOWLEDGMENTS

Funding for this research was provided by Eni S.p.A. under the Multiscale Reservoir Science Project and by the ARCO Chair in Energy Studies.

[1] M. W. Losey, M. A. Schmidt, and K. F. Jensen, Ind. Eng. Chem. Res. **40**, 2555 (2001).
[2] D. A. Dunn and I. Feygin, Drug Discov. Today **5**, 84 (2000).
[3] J. Baldyga, R. Czarnocki, B. Y. Shekunov, and K. B. Smith, Chem. Eng. Res. Des. **88**, 331 (2010).
[4] P. J. Cullen, *Food Mixing: Principles and Applications* (Wiley, 2009).
[5] J. M. Ottino and S. Wiggins, Philos. Trans. R. Soc. London A **362**, 923 (2004).
[6] H. A. Stone, A. D. Stroock, and A. Ajdari, Ann. Rev. Fluid Mech. **36**, 381 (2004).
[7] T. M. Squires and S. R. Quake, Rev. Mod. Phys. **77**, 977 (2005).
[8] M. Dentz, T. Le Borgne, A. Englert, and B. Bijeljic, J. Contaminant Hydrol. **120-121**, 1 (2011).
[9] P. Olson, P. G. Silver, and R. W. Carlson, Nature (London) **344**, 209 (1990).
[10] P. E. van Keken, E. H. Hauri, and C. J. Ballentine, Annu. Rev. Earth Planet. Sci. **30**, 493 (2002).
[11] D. Snyder and S. Tait, J. Fluid Mech. **369**, 1 (1998).
[12] O. Hallatschek and D. R. Nelson, Phys. Today **62**, 42 (2009).
[13] K. S. Korolev, M. Avlund, O. Hallatschek, and D. R. Nelson, Rev. Mod. Phys. **82**, 1691 (2010).
[14] K. R. Bhaskar *et al.*, Nature (London) **360**, 458 (1992).
[15] Y. Hatwalne, S. Ramaswamy, M. Rao, and R. A. Simha, Phys. Rev. Lett. **92**, 118101 (2004).
[16] D. Saintillan and M. J. Shelley, Phys. Rev. Lett. **100**, 178103 (2008).
[17] A. Sokolov and I. S. Aranson, Phys. Rev. Lett. **103**, 148101 (2009).
[18] A. Sokolov, R. E. Goldstein, F. I. Feldchtein, and I. S. Aranson, Phys. Rev. E **80**, 031903 (2009).
[19] K. C. Leptos, J. S. Guasto, J. P. Gollub, A. I. Pesci, and R. E. Goldstein, Phys. Rev. Lett. **103**, 198103 (2009).
[20] H. Kurtuldu, J. S. Guasto, K. A. Johnson, and J. P. Gollub, Proc. Natl. Acad. Sci. USA **108**, 10391 (2011).
[21] T. Ishikawa, N. Yoshida, H. Ueno, M. Wiedeman, Y. Imai, and T. Yamaguchi, Phys. Rev. Lett. **107**, 028102 (2011).
[22] T. H. Solomon and J. P. Gollub, Phys. Rev. A **38**, 6280 (1988).
[23] G. Boffetta, F. De Lillo, and S. Musacchio, Phys. Rev. Lett. **104**, 034505 (2010).
[24] G. M. Homsy, Ann. Rev. Fluid Mech. **19**, 271 (1987).
[25] B. Jha, L. Cueto-Felgueroso, and R. Juanes, Phys. Rev. Lett. **106**, 194502 (2011).
[26] A. R. Kopf-Sill and G. M. Homsy, Phys. Fluids **31**, 242 (1988).
[27] J. C. Bacri, N. Rakotomalala, D. Salin, and R. Woumeni, Phys. Fluids **4**, 1611 (1992).
[28] P. Petitjeans, C.-Y. Chen, E. Meiburg, and T. Maxworthy, Phys. Fluids **11**, 1705 (1999).
[29] M. A. Christie and D. J. Bond, SPE Reserv. Eng. **2**, 514 (1987).
[30] C. T. Tan and G. M. Homsy, Phys. Fluids **31**, 1330 (1988).
[31] M. A. Christie, SPE Reserv. Eng. **4**, 297 (1989).
[32] W. B. Zimmerman and G. M. Homsy, Phys. Fluids A **3**, 1859 (1991).
[33] W. B. Zimmerman and G. M. Homsy, Phys. Fluids A **4**, 1901 (1992).
[34] C.-T. Tan and G. M. Homsy, Phys. Fluids **29**, 3549 (1986).
[35] A. Riaz, C. Pankiewitz, and E. Meiburg, Phys. Fluids **16**, 3592 (2004).
[36] Y. C. Yortsos and M. Zeybek, Phys. Fluids **31**, 3511 (1988).
[37] W. B. Zimmerman and G. M. Homsy, Phys. Fluids **4**, 2348 (1992).
[38] C.-T. Tan and G. M. Homsy, Phys. Fluids **4**, 1099 (1992).
[39] H. A. Tchelepi, F. M. Orr, N. Rakotomalala, D. Salin, and R. Woumeni, Phys. Fluids A **5**, 1558 (1993).
[40] A. De Wit and G. M. Homsy, J. Chem. Phys. **107**, 9609 (1997).
[41] A. De Wit and G. M. Homsy, J. Chem. Phys. **107**, 9619 (1997).
[42] H. A. Tchelepi and F. M. Orr, SPE Reserv. Eng. **9**, 266 (1994).
[43] O. Manickam and G. M. Homsy, J. Fluid Mech. **288**, 75 (1995).
[44] E. Lajeunesse, J. Martin, N. Rakotomalala, and D. Salin, Phys. Rev. Lett. **79**, 5254 (1997).
[45] M. Ruith and E. Meiburg, J. Fluid Mech. **420**, 225 (2000).
[46] J. Fernandez, P. Kurowski, P. Petitjeans, and E. Meiburg, J. Fluid Mech. **451**, 239 (2002).
[47] A. Riaz and E. Meiburg, J. Fluid Mech. **494**, 95 (2003).
[48] J. Fernandez and G. M. Homsy, J. Fluid Mech. **480**, 75 (2003).
[49] A. De Wit and G. M. Homsy, J. Chem. Phys. **110**, 8663 (1999).
[50] A. De Wit, Phys. Rev. Lett. **87**, 054502 (2001).
[51] Y. Nagatsu, K. Matsuda, Y. Kato, and Y. Tada, J. Fluid Mech. **571**, 475 (2007).
[52] M. Mishra, M. Martin, and A. De Wit, Phys. Fluids **19**, 073101 (2007).
[53] L. Paterson, Phys. Fluids **28**, 26 (1985).

[54] H. R. Zhang, K. S. Sorbie, and N. B. Tsibuklis, Chem. Eng. Sci. **52**, 37 (1997).
[55] C. Y. Chen and E. Meiburg, J. Fluid Mech. **371**, 233 (1998).
[56] C. Y. Chen and E. Meiburg, J. Fluid Mech. **371**, 269 (1998).
[57] D. Pritchard, J. Fluid Mech. **508**, 133 (2004).
[58] C.-Y. Chen, C.-W. Huang, H. Gadêlha, and J. A. Miranda, Phys. Rev. E **78**, 016306 (2008).
[59] R. J. Blackwell, J. R. Rayne, and W. M. Terry, Petrol. Trans. AIME **217**, 1 (1959).
[60] B. Habermann, Petrol. Trans. AIME **219**, 264 (1960).
[61] E. J. Koval, Soc. Pet. Eng. J. **3**, 145 (1963).
[62] M. R. Todd and W. J. Longstaff, J. Pet. Technol. **24**, 874 (1972).
[63] F. J. Fayers, SPE Reserv. Eng. **3**, 551 (1988).
[64] F. J. Fayers, M. J. Blunt, and M. A. Christie, SPE Reserv. Eng. **7**, 195 (1992).
[65] F. J. Fayers, F. Jouaux, and H. A. Tchelepi, In Situ **18**, 43 (1994).
[66] M. Blunt and M. Christie, Transp. Porous Media **12**, 207 (1993).
[67] M. Blunt and M. Christie, SPE Advanced Technology Series **2**, 52 (1994).
[68] Z. Yang and Y. C. Yortsos, Phys. Fluids **9**, 286 (1997).
[69] E. Lajeunesse, J. Martin, N. Rakotomalala, D. Salin, and Y. C. Yortsos, J. Fluid Mech. **398**, 299 (1999).
[70] Z. M. Yang, Y. C. Yortsos, and D. Salin, Adv. Water Resour. **25**, 885 (2002).
[71] R. Juanes and M. J. Blunt, Transp. Porous Media **64**, 339 (2006).
[72] R. Juanes and M. J. Blunt, Soc. Pet. Eng. J. **12**, 486 (2007).
[73] M. Mishra, M. Martin, and A. De Wit, Phys. Rev. E **78**, 066306 (2008).
[74] S. B. Pope, *Turbulent Flows* (Cambridge University Press, Cambridge, 2000).
[75] T. Le Borgne, M. Dentz, D. Bolster, J. Carrera, J.-R. de Dreuzy, and P. Davy, Adv. Water Resour. **33**, 1468 (2010).
[76] R. J. LeVeque, *Finite Volume Methods for Hyperbolic Problems* (Cambridge University Press, Cambridge, 2002).
[77] H. Tennekes and J. L. Lumley, *A First Course in Turbulence* (The MIT Press, Cambridge, MA, 1972).
[78] N. Nakamura, J. Atmos. Sci. **53**, 1524 (1996).